

See discussions, stats, and author profiles for this publication at: <https://www.researchgate.net/publication/7761913>

Synthesis of Luminescent Silicon Nanopowders Redispersible to Various Solvents

ARTICLE *in* LANGMUIR · JULY 2005

Impact Factor: 4.46 · DOI: 10.1021/la050346t · Source: PubMed

CITATIONS

31

READS

22

3 AUTHORS, INCLUDING:



Shu-Man Liu

Chinese Academy of Sciences

31 PUBLICATIONS 448 CITATIONS

[SEE PROFILE](#)



Keisaku Kimura

Hosei University

186 PUBLICATIONS 3,755 CITATIONS

[SEE PROFILE](#)

Synthesis of Luminescent Silicon Nanopowders Redispersible to Various Solvents

Shu-man Liu, Seiichi Sato, and Keisaku Kimura*

Graduate School of Material Science, University of Hyogo, 3-2-1, Koto, Kamigori-cho, Ako-gun, Hyogo 678-1297, Japan

Received February 7, 2005. In Final Form: April 4, 2005

Silicon nanopowder with a narrow size distribution was synthesized by a simple method, in which amorphous SiO_x ($x < 2$) powder as starting material was annealed at high temperature and then etched by hydrofluoric acid (HF). Si nanoparticles thus obtained exhibited emission in the ultraviolet and visible regions under excitation at an energy corresponding to the direct band-gap transition. At the same time, they could be redispersed in various organic solvents such as octanol, toluene, etc., without surfactants or capping molecules on particle surfaces. X-ray diffraction and Fourier transform infrared spectroscopy were used to follow the change of components in the sample during annealing and HF etching processes, and the size distribution and dispersion morphology of the nanoparticles in different solvents were revealed by transmission electron microscopy analysis.

Introduction

Semiconductor nanocrystals or quantum dots have attracted more and more interest during the past decade because of their unique electronic, optical, and catalytic properties, characteristic of neither molecules (or atoms) nor solid states (bulk), among which, Si nanomaterial is currently the focus of intense research^{1–5} since Si crystal is the fundamental material for microelectronic and semiconductor industry. Differing from bulk crystalline Si that luminesce very weakly, nanocrystalline Si exhibits intense luminescence over the visible spectra region^{6–20} and is expected to introduce new functionality in the field of optoelectronic devices.

Si nanocrystals have been fabricated by various techniques, such as thermal evaporation,^{11,12} laser ablation,¹³ pyrolysis of silane,¹⁴ Si ion implantation into SiO_2 film

followed by high-temperature annealing,¹⁵ sputtering,^{16,17} electrochemical etching of Si wafers,¹⁸ etc.. Although great progress on well-defined Si nanostructures has been achieved by the above methods, there still remains a highly arduous challenge to find a simple and mild production route to synthesize chemically stable, size uniform, and well dispersed Si nanoparticles, which is of great benefit for further building and patterning of the nanoparticles into organized structures.^{19–22} Recently, there has been some advancement in wet chemical synthesis methods for Si semiconductor nanocrystals that can be dispersed in organic solvents due to surface modification by organic molecules. For instance, organic soluble Si nanoparticles have been synthesized by reduction of SiCl_4 by reagents such as anhydrous metal hydride,²³ metal silicides,²⁴ or naphthalide salts²⁵ in strictly anhydrous organic solvents.

Si-rich silicon suboxide films have been used as semi-insulating polysilicon films in Si-based electronic devices. Such films are generally annealed in the course of their processing, and formation of Si clusters during annealing has been reported in the past decades.^{26–29} But the size distribution and distribution density of the Si clusters embedded in the annealed films cannot be adjusted easily. In the previous work of our group, a simple method to prepare Si nanoparticles suspended in solution was proposed, in which commercially available SiO_x suboxide powder was etched by HF and then hydrogenated Si particles were left suspended in solution.³⁰ This approach allowed formation of Si nanoparticles with narrow size distribution, but too low yield of products made it very

- * To whom correspondence should be addressed. Tel: 81-791-58-0159, Fax: 81-791-58-0161, E-mail: kimura@sci.u-hyogo.ac.jp.
- (1) Alivisatos, A. P. *Science* **1996**, *271*, 933.
- (2) Bruchez, M.; Moronne, M.; Gin, P.; Weiss, S.; Alivisatos, A. P. *Science* **1998**, *281*, 2013.
- (3) Rao, C. N. R.; Cheetham, A. K. *J. Mater. Chem.* **2001**, *11*, 2887.
- (4) Wang, Z. L. *J. Phys.: Condens. Matter* **2004**, *16*, R829.
- (5) Brunner, K. *Rep. Prog. Phys.* **2002**, *65*, 27.
- (6) Canham, L. T. *Appl. Phys. Lett.* **1990**, *57*, 1046.
- (7) Meindl, J. D.; Chen, Q.; Davis, J. A. *Science* **2001**, *293*, 2044.
- (8) Cui, Y.; Lieber, C. M. *Science* **2001**, *291*, 851.
- (9) Ding, Z.; Quinn, B. M.; Haram, S. K.; Pell, L. E.; Korgel, B. A.; Bard, A. J. *Science* **2002**, *296*, 1293.
- (10) Morales, M.; Lieber, C. M. *Science* **1998**, *279*, 208.
- (11) van Buuren, T.; Dinh, L. N.; Chase, L. L.; Siekhaus, W. J.; Terminello, L. J. *Phys. Rev. Lett.* **1998**, *80*, 3803.
- (12) Iwasaki, S.; Kimura, K. *Mater. Res. Soc. Symp. Proc.* **1997**, *272*, 165.
- (13) Seraphin, A.; Ngiam, S.-T.; Kolenbrander, K. D. *J. Appl. Phys.* **1996**, *80*, 6429.
- (14) Ledoux, G.; Gong, J.; Huisken, F. *Appl. Phys. Lett.* **2001**, *79*, 4028.
- (15) Brongersma, M. L.; Kik, P. G.; Polman, A.; Min, K. S.; Atwater, H. A. *Appl. Phys. Lett.* **2000**, *76*, 351.
- (16) Zhu, Y.; Kimura, K.; Zhang, L. D. *J. Vac. Sci. Technol.* **1997**, *B15*, 2077.
- (17) Dovrat, M.; Goshen, Y.; Jedrzejewski, J.; Balberg, I.; Sa'ar, A. *Phys. Rev. B* **2004**, *69*, 155311.
- (18) Yamani, Z.; Thompson, W. H.; Abuhassan, L.; Nayfeh, M. H. *Appl. Phys. Lett.* **1997**, *70*, 3404.
- (19) Murray, C. B.; Kagan, C. R.; Bawendi, M. G. *Science* **1995**, *270*, 1335.
- (20) Granot, E.; Patolsky, F.; Willner, I. *J. Phys. Chem. B* **2004**, *108*, 5875.

- (21) Milliron, D. J.; Hughes, S. M.; Cui, Y.; Manna, L.; Li, J.; Wang, L. W.; Alivisatos, A. P. *Nature* **2004**, *430*, 190.
- (22) Jana, N. R. *Angew. Chem., Int. Ed.* **2004**, *43*, 1536.
- (23) Wilcoxon, J. P.; Samara, G. A.; Provencio, P. N. *Phys. Rev. B* **1999**, *60*, 2704.
- (24) Yang, C.; Bley, R. A.; Kauzlarich, S. M.; Lee, H. W. H.; Delgado, G. R. *J. Am. Chem. Soc.* **1999**, *121*, 5191.
- (25) Baldwin, R. K.; Pettigrew, K. A.; Ratai, E.; Augustine, M. P.; Kauzlarich, S. M. *Chem. Commun.* **2002**, 1822.
- (26) Nesbit, L. A. *Appl. Phys. Lett.* **1985**, *46*, 38.
- (27) Choi, W. C.; Lee, M.; Kim, E. K.; Kim, C. K.; Min, S.; Park, C.; Lee, J. Y. *Appl. Phys. Lett.* **1996**, *69*, 3402.
- (28) Yun, F.; Hinds, B. J.; Hatatami, S.; Oda, S.; Zhao, Q. X.; Willander, M. *Thin Solid Film* **2000**, *375*, 137.
- (29) Khriachtchev, L.; Rasanen, M.; Novikov, S.; Pavesi, L. *Appl. Phys. Lett.* **2004**, *85*, 1511.
- (30) Sato, S.; Yao, H.; Kimura, K. *Jpn. J. Appl. Phys.* **2004**, *43*, L927.

difficult to understand their electronic and optical properties comprehensively and in-depth.

In the present study, first, an improved wet synthesis route to give a large quantity of Si nanopowder is proposed. Then structure and photoluminescence properties are discussed. Finally, the redispersibility of the nanopowder in liquid medium is discussed.

Experiment Section

Preparation of Si Nanoparticles. Si nanoparticles were synthesized by using silicon suboxide (SiO_x , x from 0.4 to 1.8) powder supplied by DENKA Co. as the starting material. First, SiO_x powders were annealed at high temperature of 900 °C for 1 h under a flow of Ar gas at ambient atmosphere. For this annealing treatment, a quartz tube was set horizontally inside a high-temperature resistance furnace. SiO_x powders were put into a ceramic crucible, which was placed in the center of the tube. Then the tube was sealed after evacuated to 0.3 kPa, and the furnace was heated at a rate of 30 °C/min to the desired temperature and maintained for 1 h. During the annealing process, a pure Ar flow at a flow rate of 1.0 L/min was continuously introduced through the quartz tube and the pressure within the tube was maintained at ~1 atm. Annealing at 1100 °C was conducted in a muffle with firebrick lining for comparison, in which the SiO_x powders were put into a refractory crucible. Also a pure Ar flow at the same flow rate was introduced through the furnace chamber, but which cannot be evacuated before introduction of Ar flow. Then annealed SiO_x powders were suspended in methanol. Usually mild ultrasonic treatment was enough to obtain better dispersion of the suspension. To the suspension, a HF aqueous solution (1–5%) was added to dissolve the silicon dioxide in annealed powders. Our experiments were conducted on SiO_x powders with 10 different x values from 0.35 to 1.81. Here we show representative results of $x = 1.6, 1.0, and 0.4, because the starting materials with an x value from 1.5 to 1.81 resulted in similar particle size and showed similar luminescent properties to $\text{SiO}_{1.6}$ after the same thermal annealing and acid etching processes. SiO_x powders with x between 0.8 and 1.19 analogously showed similar results to $\text{SiO}_{1.0}$ after annealing and etching treatments, and SiO_x with x between 0.35 and 0.69 behaved similar to $\text{SiO}_{0.4}$ during the annealing and etching.$

To obtain dry powders of sample after HF etching, particles were collected on polyvinylidene fluoride (PVDF) membrane filters (Millipore) from the suspensions and washed with distilled water and methanol. The washed particles on membrane filters were redispersed in methanol with the help of sonic oscillation, concentrated by using a rotary evaporator, and then vacuum-dried at room temperature.

Instruments and Characterization. X-ray diffraction (XRD) measurements of annealed and etched powders were carried out on a Rigaku Rint 2000 diffractometer with Cu K α radiation ($\lambda = 1.5418 \text{ \AA}$) operated at 40 kV and 20 mA. Annealed powders and etched particles collected on membranes were used for XRD measurements.

Fourier transform infrared (FT-IR) spectra were measured with a Horiba FT-210 infrared spectrophotometer using a 150 mg KBr disk dispersed with the dry SiO_x or Si particles at a weight ratio of about 0.5%. The background correction was conducted by using a reference "blank" KBr pellet.

A Hitachi-8100 transmission electron microscope (TEM), operated at 200 kV with 2.1 Å point-to-point resolution, was used to measure the size and analyze the structure and morphology of Si nanoparticles. For the specimen preparation, powder sample was redispersed in methanol, water, *n*-octanol, and toluene, respectively. Then the suspension was dropped on an amorphous carbon-coated Cu grid and dried in a vacuum desiccator for 12 h. The histograms of the nanocrystals were obtained by measuring the diameter of particles with a NIH Image 1.30v software package. The number of particles measured is about 400. The standard deviation, σ , was calculated from the experimentally determined distributions:

$$\sigma = [\sum (D_i - D)^2 / (n - 1)]^{1/2}$$

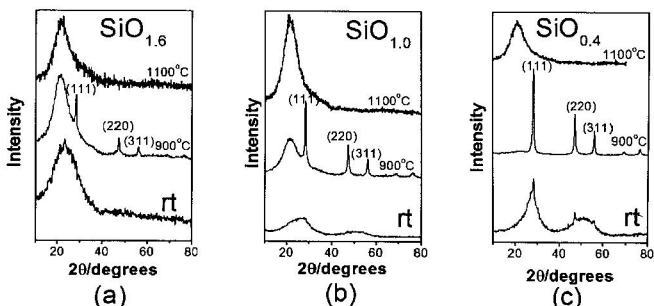


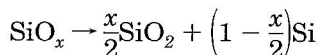
Figure 1. XRD patterns of as-received (labeled by room temperature) and annealed SiO_x powder. The x value is (a) 1.6, (b) 1.0, and (c) 0.4, respectively, and the annealing temperature has been indicated in the figure.

where D_i is the diameter of the measured particle, n is the number of particles measured, D is the average diameter, and the polydispersity is defined as the ratio σ/D .³¹

Photoluminescence (PL) spectra were recorded with a Hitachi F-4500 fluorescence spectrophotometer. The Si particle suspensions were excited by a 150 W xenon lamp. The excitation wavelength was set to 355 nm and the emission cutoff filter was set to 370 nm for all the measurements shown hereafter.

Results and Discussion

Crystallization Induced by Annealing and Effect of Etching on Silicon Suboxides. The XRD patterns of three starting materials shown in Figure 1 (patterns at bottom labeled as room temperature) indicate their amorphous characteristics with x values in the range between 0.4 and 1.6, among which $\text{SiO}_{1.6}$ consists of amorphous Si oxide phase while $\text{SiO}_{0.4}$ and $\text{SiO}_{1.0}$ powders contain mainly Si phase with poor crystallization. It has been reported^{27,28} that high-temperature annealing of amorphous SiO_x films at 1100 °C resulted in phase separation following the reaction of



Our annealing experiments show that high temperature of 1100 °C thermal treating of the starting materials in Ar atmosphere result in deep oxidation of amorphous SiO_x powders. As shown in Figure 1, the XRD patterns for the three 1100 °C annealed samples are dominated by the SiO_2 amorphous phase according to JCPDF card (No.29-85). There is no detectable signal from the Si phase for all three x values. Since air or oxygen cannot be excluded from our muffle furnace completely, we believe that our annealing at 1100 °C for 1 h resulted in the deep oxidation of SiO_x powders. Meanwhile our previous work indicated that there remained nanosized Si particles with good crystallization after 1100 °C annealing,³⁰ but the diffraction peaks of Si phase in the annealed samples were masked due to less amounts of Si particles. Therefore in the present work, a lower annealing temperature was adopted and large quantities of Si particles were obtained as indicated by the XRD patterns of 900 °C annealed samples. It is clear that the phase separation following the above reaction has taken place during annealing at 900 °C for 1 h and resulted in formation of crystallized Si particles (indicated by narrow diffraction peaks) and amorphous SiO_2 phase (wide diffraction peak at 2θ of 21°) from the initial amorphous suboxides. Further, the XRD results show different ratios of Si to SiO_2 for the three samples, i.e., the $\text{SiO}_{1.6}$ results in more oxide phase than silicon one, $\text{SiO}_{1.0}$ leads to almost the same quantity of

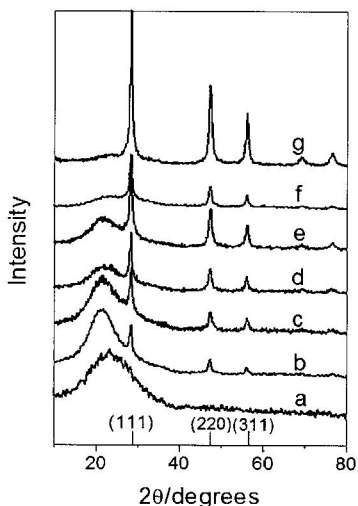


Figure 2. The change of XRD patterns during HF etching process. Curves a and b were measured on $\text{SiO}_{1.6}$ starting material and 900 $^{\circ}\text{C}$ annealed sample, respectively. Curves c–g were obtained after etching for (c) 1 h, (d) 2 h, (e) 3 h, (f) 4 h, and (g) 6 h.

oxide and Si phase, while the Si-rich starting material $\text{SiO}_{0.4}$ produces a large amount of Si crystallites and few oxides, which is consistent with the above reaction equation.

We will show the effect of HF etching as verified by the evolution of XRD patterns. Neglecting the different relative content of the Si phase, the three samples behave very similarly during HF etching. Here the result of $\text{SiO}_{1.6}$ shown in Figure 2 is discussed as a representative example. Patterns a and b due to the as-received and 900 $^{\circ}\text{C}$ annealed samples, respectively, are also provided in the figure for a convenient comparison. From pattern c to g, the oxide phase decreases with the etching time and almost disappears after 6 h etching. An average size of 14 nm is estimated from XRD pattern g using the Scherrer formula, which is much larger than that obtained from direct TEM observation. Since a very small amount of precipitate can be found at the bottom while most particles are dispersed well in the solvent during the preparation of TEM sample described in the Experimental Section, we consider that the diffraction is dominated by the minority of large crystallites.

Also it must be pointed out that when following the change of the sample during etching by FT-IR measurements, we found that there still exist strong Si–O vibration modes even after HF etching for 10 h. The FT-IR spectra a–e shown in Figure 3 were measured on as-received $\text{SiO}_{1.6}$ powder, 900 $^{\circ}\text{C}$ annealed sample, and samples at several stages during HF etching, respectively. The strong peak at about 1100 cm^{-1} in curves a–d is the characteristic of Si–O stretch vibration, the vibrations between 520 and 750 cm^{-1} in curve e are due to Si–H₂ scissors or Si–H₃ symmetric or antisymmetric deformation modes, the weak peaks between 880 and 900 cm^{-1} are due to Si–H wagging vibration, and the peaks between 2050 and 2300 cm^{-1} result from Si–H stretching mode.³² We can see that etching by 1% HF for 1 day (curve e) can remove silicon oxide in the annealed powders and cover the particle surface with Si–H components.

Formation of Si Nanoparticles and Their Photoluminescence. The acid-etched sample was redispersed in methanol and dropped on a Cu grid coated by an

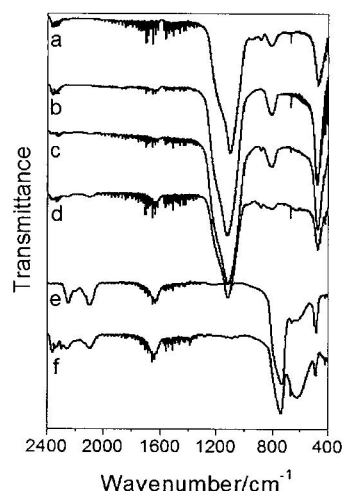


Figure 3. FT-IR spectra recorded on (a) $\text{SiO}_{1.6}$ starting material, (b) 900 $^{\circ}\text{C}$ annealed sample, samples after 1% HF etching for (c) 5 h, (d) 10 h, (e) 1 day, and (f) the sample after HF– HNO_3 etching for 1 h.

amorphous carbon film for TEM observation. Figure 4a shows the TEM image and corresponding histogram of a typical sample which was etched by 1% HF for 1 day. The image shows clearly the formation of spherical particles. The average size of the particles is 4.2 nm with the polydispersity of 12%. The formation of Si nanoparticles is further confirmed by high-resolution transmission electron microscopy (HRTEM) measurement. Figure 4b shows an isolated large particle in diameter of ~ 10 nm, in which the lattice fringes with d spacing of 0.31 nm are consistent with the {111} crystal plane of diamond structured Si.

During the HF etching process, the oxide as indicated by the wide peak at 21° (curve b in Figure 2) was etched by HF, leaving the Si nanocrystallites suspended in solution with Si–H surface modification. It is a common knowledge that Si itself can hardly react with HF; therefore, only the oxide product during annealing is etched and removed by HF, and the average size of Si particles after HF etching should be equal to that before etching. This should be indicated by XRD patterns c–g in Figure 2, i.e., the width of diffraction peaks should scarcely change during HF etching within 6 h. But as discussed above, the sharp peaks result from a minority of large crystallites; thus, it can hardly elucidate the complicated evolution of the majority of small particles during etching only by XRD. It has been known that small Si particles tend to form oxide on particle surfaces when exposed to air even at room temperature; hence, longer etching time and ultrasonic oscillation should facilitate the formation of such oxide at surface, which was then etched by HF. The oxidization and etching process resulted in smaller Si nanoparticles in the sample. Li et al. have reported³³ that etching on Si nanoparticles using a mixture of HF and HNO_3 was rather fast. Their starting Si nanoparticles were produced by laser pyrolysis of silane. For comparison with the HF etching route, a mixture of HF (1–5%) and HNO_3 (2–20%) was also used to etch our annealed SiO_x powders. Figure 5 shows the TEM image with its size distribution of the sample etched by the mixture of 2% HF and 10% HNO_3 for 1 h, and its FT-IR spectrum is shown in Figure 3f. The average size of the obtained particles is 3.7 nm with a polydispersity of $\sim 17\%$. As seen from Figure 3, the FT-IR spectrum f is identical to that of 1-day HF-

(32) Belomoin, G.; Therrien, J.; Nayfeh, M. *Appl. Phys. Lett.* **2000**, 77, 779.

(33) Li, X.; He, Y.; Swihart, M. T. *Langmuir* **2004**, 20, 4720.

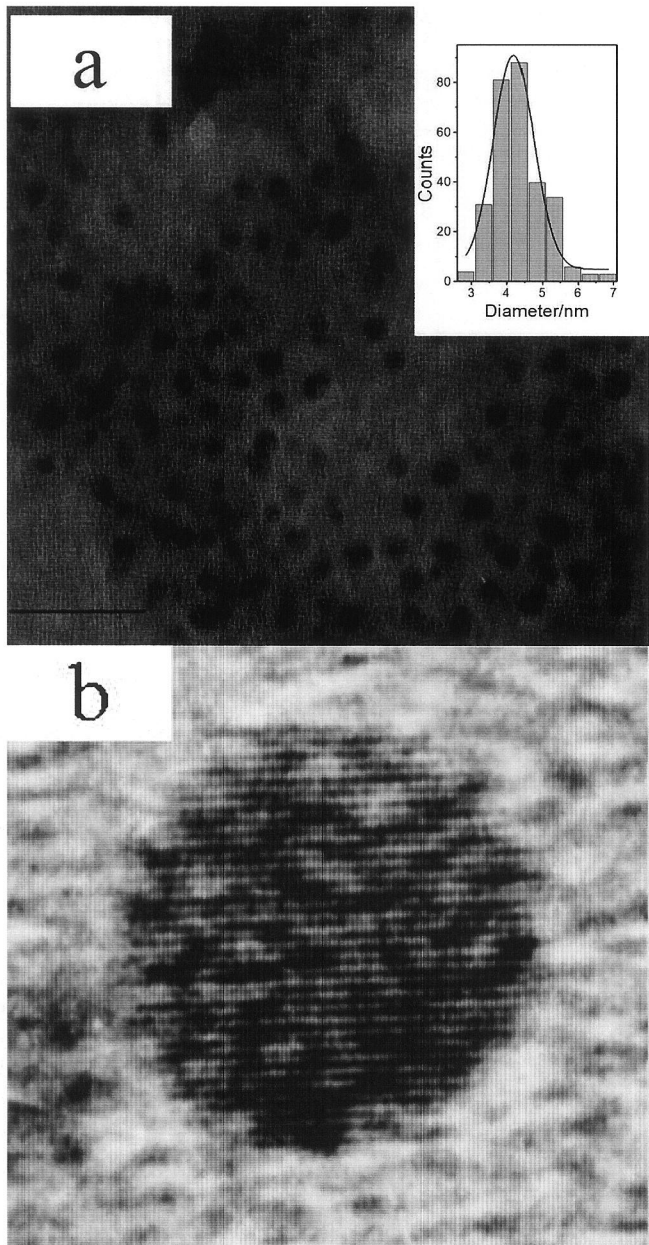


Figure 4. (a) TEM image of HF-etched sample and the size distribution with Gaussian line shape fit from 400 particles and (b) HRTEM image of an isolated Si particle. The bar at the bottom of part a is 22 nm, and the fringe lattice d spacing in part b is 0.31 nm.

etched sample (curve e), i.e., silicon oxide has been almost removed and Si–H bond dominated on particle surfaces. From our experiment, addition of HNO_3 also accelerated the etching process, but the problem at this time is the difficulty in collecting enough powder samples. It has been noticed that our starting material is SiO_x suboxide powder, which probably resulted in a too rapid etching rate in the presence of HNO_3 in our case. Thus, it is the rather slow reaction by using HF only etching that makes the mass-production possible. Moreover, Iijima et al. have reported that the oxide growth rate on small Si particles decreases with decreasing particle size.³⁴ Here our result coincides with their observation. During the slow HF etching and air oxidation processes described above, larger particles were oxidized more quickly and then reduced their size faster than smaller ones, which finally led to narrow size distribution of the Si nanoparticles.

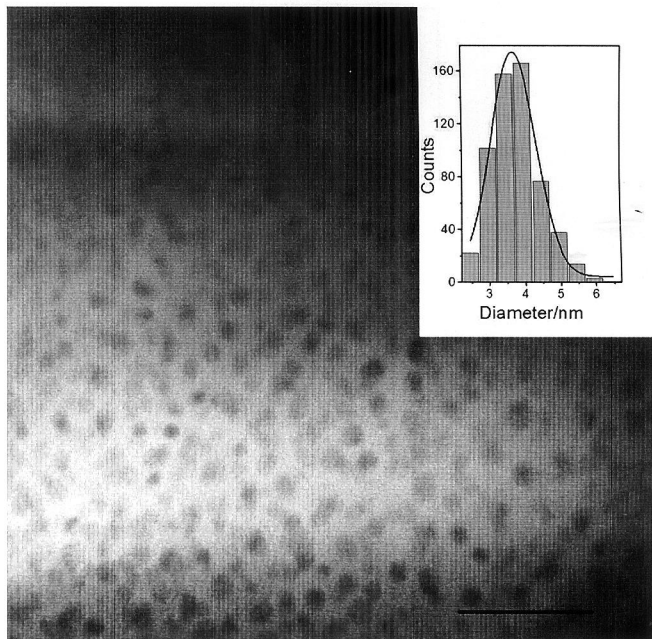


Figure 5. TEM image of HF– HNO_3 -etched sample and the size distribution with Gaussian line shape fit from 500 particles. The bar at the bottom is 22 nm.

Upon annealing starting materials at 900 °C, the Si particles show little luminescence with irregular structures. Very similar visible photoluminescence was obtained after etching the 900 °C annealed $\text{SiO}_{1.6}$ and $\text{SiO}_{1.0}$ by HF acid. No emission can be detected from 900 °C annealed $\text{SiO}_{0.4}$ even after etching by HF; thus, controlled thermal oxidation of this sample before acid etching is under investigation to obtain luminescent Si particles. Here the result of $\text{SiO}_{1.6}$ is discussed as follows.

Under UV excitation from 254 nm to 400 nm, the annealed powders before HF etching usually exhibit a weak wide emission band from 400 to 700 nm with irregular structure. On the other hand, no emission can be detected when excited by low energetic photons located between 400 nm to 500 nm. Since UV excitation energy corresponds to direct band gap absorption in medium sized Si nanoparticles (4–10 nm),²³ upon irradiation with the UV photons, excited carriers due to direct band gap absorption are prone to relax into many kinds of states with lower energy, such as indirect band edge, unsaturated Si atoms on surfaces, or other defects existing in Si cores, Si/oxide interfaces, or oxide phases.^{35,36} As shown by XRD patterns in Figure 1, our annealed powders consist of amorphous silicon oxides and Si particles. A large amount of defects are supposed to exist in these materials. Even if a few optical active sites such as perfect Si nanoparticles or some Si–O specimens^{36,37} make the lower energy emission possible, many optical inactive sites lead to nonradiative relaxation and suppress the emission from these samples.

After etching in HF for 1 day, the sample luminesces in the visible range. Figure 6a shows the evolution of the PL emission spectrum with time after etching in HF. Freshly etched sample within 6 h emits at 520 nm and 397 nm. After 10 h and 1 day, the visible emission band at 520 nm blue-shifts to 502 nm and 487 nm, respectively,

(34) Okada, R.; Iijima, S. *Appl. Phys. Lett.* **1991**, *58*, 1662.

(35) Garrido, B.; M. Lopez., Gonzalez, O.; Perez-Rodriguez, A.; Morante, J. R. *Appl. Phys. Lett.* **2000**, *77*, 3143.

(36) Kimura, K.; Iwasaki, S. *J. Appl. Phys.* **1998**, *83*, 1345.

(37) Kanemitsu, Y.; T. Futagi., Matsumoto, T.; Mimura, H. *Phys. Rev. B* **1994**, *49*, 14732.

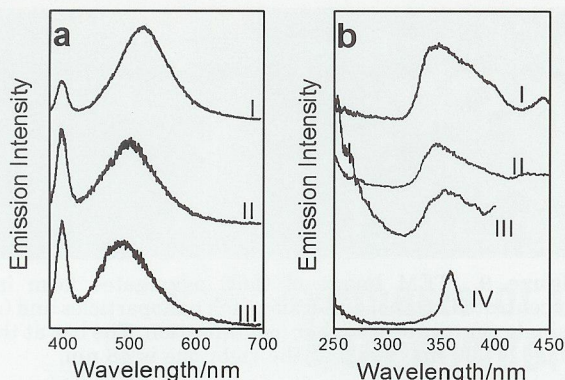


Figure 6. (a) PL spectra of sample after HF etching for (I) 3 h, (II) 6 h, and (III) 1 day recorded by excitation at 355 nm wavelength; (b) PLE spectra recorded at detection wavelength of (I) 520 nm, (II) 502 nm, (III) 487 nm, and (IV) 400 nm. Spectra I and IV were recorded on sample after HF etching for 3 h, spectra II and III were recorded on sample after HF etching for 6 h and 1 day, respectively.

while the high energy emission stays at 397 nm after 1 day. The full width at half-maximum (fwhm) of the band in the visible range is 80 nm (0.4 eV) for curves I–III, while the emission band at 397 nm is narrow with the fwhm of 15 nm (0.12 eV). To elucidate the origin of the emission, photoluminescence excitation (PLE) spectra were recorded as shown in Figure 6b. It suggests that the two emission bands resulted from photon absorption near 355 nm (3.54 eV). The average particle size of the present sample is about 4 nm from the TEM observation. The direct band gap at Γ ($\Gamma_{25}-\Gamma_{15}$) of this size of Si particle is 3.5 eV.²³ Thus the optical absorption at 350 nm in PLE spectra results in carrier transition in Si cores at Γ point. PL bands located between 450 nm and 650 nm have been reported as emission from relaxed electron–hole pairs at some emissive centers located at interface of Si/SiO₂ or interior of oxide layer and do not shift with particle size.³⁸ In our case, the narrow PL peak at 400 nm shows no change with etching time within 1 day but disappears after a long period of more than 2 days. So we suppose an exogenous origin of this narrow PL peak, whose corresponding emissive centers turn into nonradiative ones after the long aging of the particles during the etching process. The wide emission band in the visible range increases its energy with etching time first quickly and then stays at 460 nm for several days. Many previous studies have reported a red emission from ~4 nm sized Si nanoparticles and ascribed it to radiative recombination of e–h pairs at the enlarged band-gap due to quantum confinement. Since most samples were Si nanocrystals capped with SiO₂ or embedded in glasses except several organic soluble Si nanoparticles,^{23,24,33,39} we compare our results with those in organic solution and know that the visible emission from our sample is consistent to a certain extent with the PL centered at 520 nm observed by Korgel³⁹ from organic-monolayer passivated Si nanocrystals at a size of 2.5–4 nm, and the PL between 315 and 520 nm for alkyl-terminated Si nanoclusters with an average size of 2–5 nm reported by Kauzlarich.²⁴ Thus we prefer to describe the PL origin as an innate native character of Si particles since the peak position shifts to high energy with the decreasing particle size. However, we notice the average size of 4.2 nm from our TEM observation is somewhat larger than that reported in the two previously

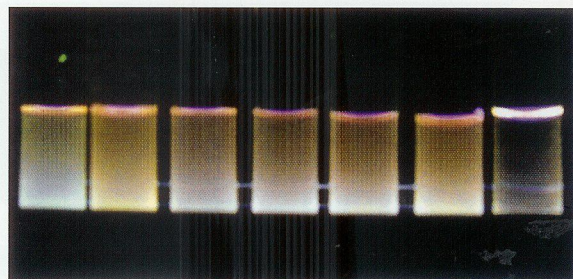


Figure 7. Samples dispersed in various solvents and illuminated by an UV lamp with 254 nm wavelength. From left to right the solvent is octanol, toluene, methanol, chloroform, acetonitrile, DMF, and hexane, respectively. Homogeneous dispersions are obtained for all the solvents except the case of hexane, in which sample precipitated quickly.

cited reports; thus, it might be possible that particles much smaller than 4.2 nm also contribute to the visible emission between 460 nm and 520 nm in our sample. Meanwhile, we will not exclude an extrinsic origin of the visible emission in our sample, as the PL mechanism is still the topic of debate and further investigation is needed for our sample.

Dispersion and Aggregation of Si Nanoparticles in Different Solvents. Hydrogenated Si nanoparticles tend to aggregate quickly when dispersed in water due to the hydrophobic Si–H on particles surfaces.³⁰ To investigate the dispersion characteristics in solvents with different molecular composition and polarity, we dispersed the above hydrogenated Si particles in water, methanol, octanol, toluene, chloroform, dimethylformamide (DMF), and hexane with the same low concentration of 0.01 mg/mL, respectively. An almost transparent Si nanoparticle suspension was formed in methanol, octanol, toluene, chloroform, and DMF. Conversely, only a few particles were dispersed in water while most of them agglomerate and floated on water surface. A drop of bulk aqueous suspension was adopted for TEM observation. In the case of hexane, the particles precipitated very soon after ultrasonic dispersion.

First, a digital photograph is shown in Figure 7 to illustrate the dispersibility of the Si nanopowder in different solvents directly. Note that whole bulk solution luminescence suggests that a homogeneous dispersion system has been obtained in octanol, toluene, methanol, chloroform, acetonitrile, and DMF, while there is no emission from the hexane system since Si particles precipitated at the bottom. It was also reported⁴⁰ that Si nanoparticles fabricated by laser ablation adsorbed on CH₃-terminated self-assembled monolayer (SAM) while they did not adsorb on NH₂, F, OH, and COOH-terminated SAM in the evaporation chamber. But our dispersion experiments were conducted in solution. It seems that the CH₃ group does not dominate the dispersity of Si particle with hydrogenated surfaces in solvents, since hexane is not a good dispersing medium in our case. Then dispersive states of Si nanoparticles deposited from several solvents was observed from TEM measurements. Figure 8 shows the TEM images of the four suspensions of Si nanopowders, which show different distribution morphology. Particles deposited from methanol suspension distribute randomly as shown in Figure 8a. Figure 8b shows obvious agglomeration of particles dispersed in water. In Figure 8c, particles distribute rather isolatedly, while particles from toluene suspension appear condensed as in

(38) Kimura, K.; Iwasaki, I. *Jpn. J. Appl. Phys.* **1999**, *38*, 609.

(39) Holmes, J. D.; Ziegler, K. J.; Christopher Doty, R.; Pell, L. E.; Johnston, K. P.; Korgel, B. A. *J. Am. Chem. Soc.* **2001**, *123*, 3743.

(40) Hata, K.; Fujita, M.; Yoshida, S.; Yasuda, S.; Makimura, T.; Murakami, K.; Shigekawa, H. *Appl. Phys. Lett.* **2001**, *79*, 692.

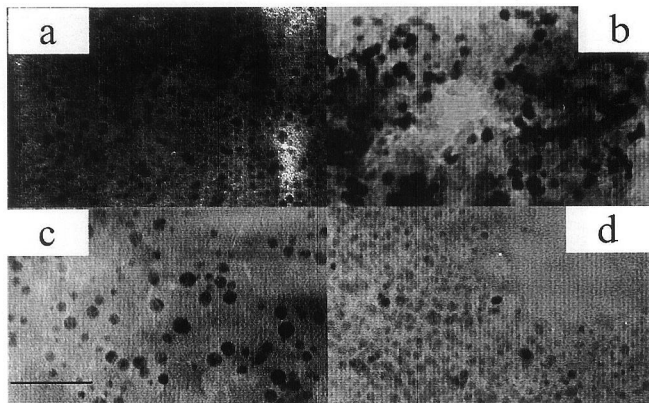


Figure 8. TEM images of Si particles dispersed in (a) methanol, (b) water, (c) octanol, and (d) toluene. The bar is 33 nm common for all figures.

Figure 8d. It is known that the drying process depends on many parameters such as the solvent vapor pressure, surface tension, surface energy of the grid coating/solvent interface, etc. L. E. Brus's group has reported that different solvent evaporation rates of octane, chloroform, and hexane resulted in different self-assembly of semiconductor nanoparticles on the HOPG surface, as the viscosity coefficients of these solvents are very close at room temperature.^{41,42} In our experiment, the viscosity of octanol is much larger (8.2 mPa·S) than that of methanol (0.597 mPa·S) and toluene (0.586 mPa·S), so both the viscosity and the evaporation rate of the solvent should be considered according to their model. Furthermore, more Si nanoparticles (0.1 mg/mL) were dispersed in octanol and toluene for the investigation by using TEM. Toluene suspension with a higher concentration of Si particles shows a dense distribution similar to the diluted one. On the other hand, the concentrated octanol suspension presents different particle distribution morphology as shown in Figure 9. The left image contains a large number of aggregates with an average size of ~66 nm. The right one gives an enlarged image of one aggregate. It is obvious that the Si particles have self-assembled into large aggregates. A further investigation of the octanol dispersion of hydrogenated Si nanoparticles is in progress to clarify the interaction between octanol molecules and

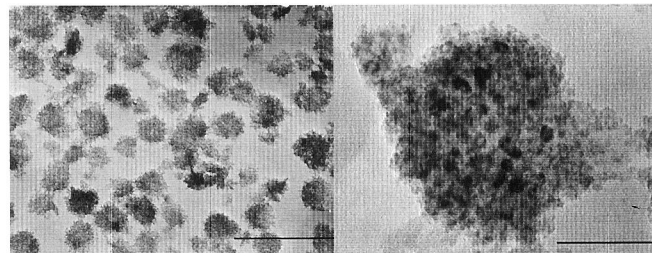


Figure 9. TEM image of (left) aggregates form in the concentrated octanol dispersion of Si nanoparticles and (right) a single aggregate at higher magnification. The bar at the left image is 290 nm, while at the right one is 48 nm.

Si nanoparticles and, furthermore, to assemble the Si particles into more ordered structures.

Conclusion

In summary, Si nanoparticles were prepared through annealing and subsequent etching with HF from amorphous SiO_x ($x < 2$) powders as starting materials. Due to the rather slow etching process, a narrow size distribution of 12% in polydispersity obtained by TEM observation was achieved for a typical sample. Photoluminescence from UV to the visible region under excitation at the energy corresponding to direct band gap transition was observed from HF-etched samples. TEM observation shows different disperse morphology of Si particles when dispersed in different solvents, i.e., in the case of low concentration, they distribute randomly with inhomogeneous distance in methanol, scatter isolatedly with very large distance in octanol, and arrange densely in toluene. Especially, when suspended in octanol at a high concentration, Si particles tend to self-assemble into large aggregates in the size of ~66 nm. We believe the redispersibility of Si nanopowders in various solvents is of great benefit to the assembly of Si nanoparticles into more ordered nanostructures, which could provide potential applications such as optoelectronic and nanoelectronic devices.

Acknowledgment. Financial support and granting of the postdoctoral fellowship (P03278, #15.03278) of this work from the Japan Society for Promotion of Science is gratefully acknowledged. This work is also supported in part by Grant-in-Aid for Scientific Research (S: 16101003). We are also indebted to Mrs. Y. Imamura and T. Kawasaki of DENKA Co. Ltd. for supplying various kinds of SiO_x samples.

LA050346T

(41) Tang, J.; Ge, G.; Brus, L. E. *J. Phys. Chem. B* **2002**, *106*, 5653.

(42) Rabani, E.; Reichman, D. R.; Geissler, P. L.; Brus, L. E. *Nature* **2003**, *426*, 271.